# Supplementary Information

**From fluorene molecules to ultrathin carbon nanonets with enhanced charge transfer capability for supercapacitors**

Xiaojun He[a,*], Xiaoyu Xie[a], Jingxian Wang[a], Xiufang Ma[b], Yuanyang Xie[a], Jing Gu[a], Nan Xiao[c], Jieshan Qiu[d,*]

**Figure captions**

**Figure S1.** (a) TEM image of sheet-like MgO particles. (b, c) Size of MgO particles.

**Figure S2.** TEM images of (a, b) $UCN^0_{0\text{-}10}$. $UCN^0_{0\text{-}10}$ is made on 2 g naked nano-MgO particles in another corundum boat.

**Figure S3.** Schematic for the relative position of corundum boats in horizontal tubular furnace.

**Figure S4.** $N_2$ adsorption-desorption isotherms of: (a) $UCN_{0\text{-}10}$, (c) $UCN_{3\text{-}0}$. Pore size distribution curves of: (b) $UCN_{0\text{-}10}$, (d) $UCN_{3\text{-}0}$. (e) XRD patterns of $UCN_{0\text{-}10}$ and $UCN_{2\text{-}10}$. (f) Raman spectra of $UCN_{0\text{-}10}$ and $UCN_{2\text{-}10}$.

**Figure S5.** Carbon nanonets from fluorene molecules via step-by-step self-assembly process.

**Figure S6.** Schematic for the step-by-step assembly of six-membered fluorene rings.

**Figure S7.** Schematic for the assembly of UCN from fluorene molecules.

**Figure S8.** Schematic for the assembly of UCNs from fluorene molecules in nano-MgO-template-confinement space with the aid of KOH.

**Figure S9.** (a) CV curves of $UCN_{3\text{-}10}$ electrode at 2 and 5 mV $s^{-1}$. (b) CV curves of $UCN_{0\text{-}10}$ electrode at 2 and 5 mV $s^{-1}$.

**Table captions**

**Table S1** The pore structure parameters of UCN samples.

**Table S2** The XPS results of the UCN samples.

**Table S3** Comparison of the specific capacitance of the UCN electrode with that of the hollow nanostructure carbons.

**Table S4** Comparison of the performance of the UCN electrode with that of the carbon-based electrode materials.

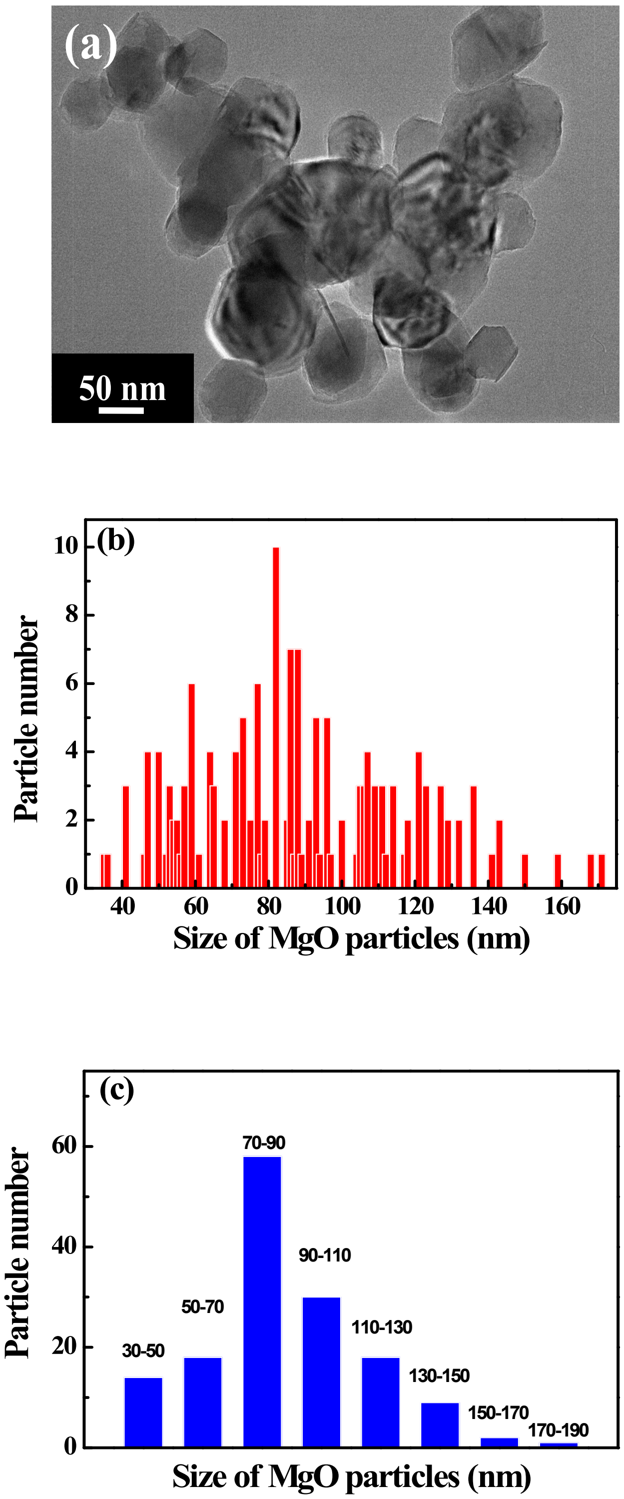


**Figure S1.** (a) TEM image of sheet-like MgO particles. (b, c) Size of MgO particles.

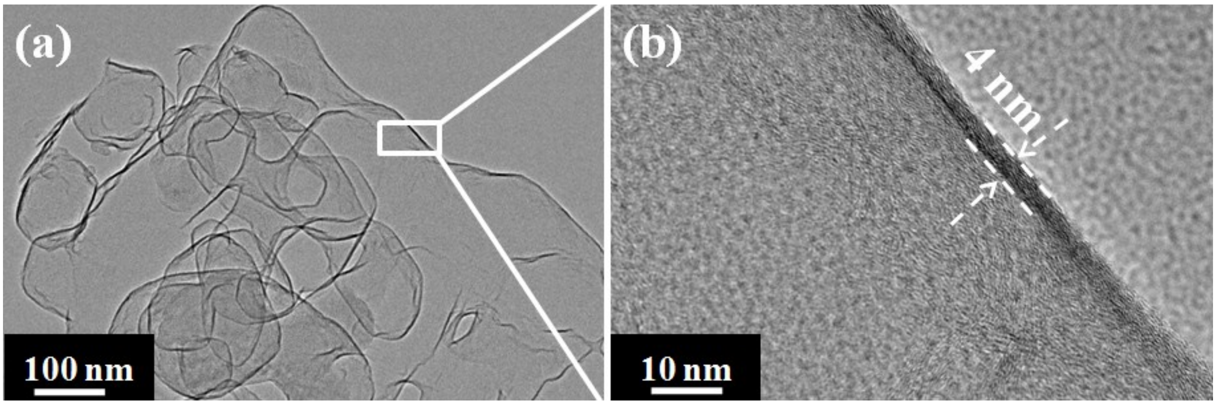


**Figure S2.** TEM images of (a, b) $UCN^0_{0\text{-}10}$. $UCN^0_{0\text{-}10}$ is made on 2 g naked nano-MgO particles in another corundum boat.

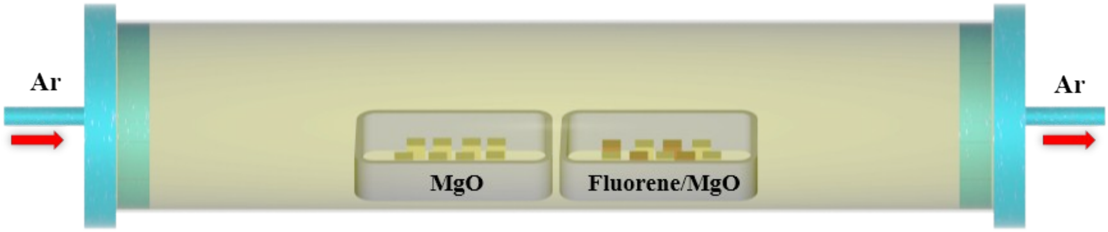


**Figure S3.** Schematic for the relative position of corundum boats in horizontal tubular furnace.

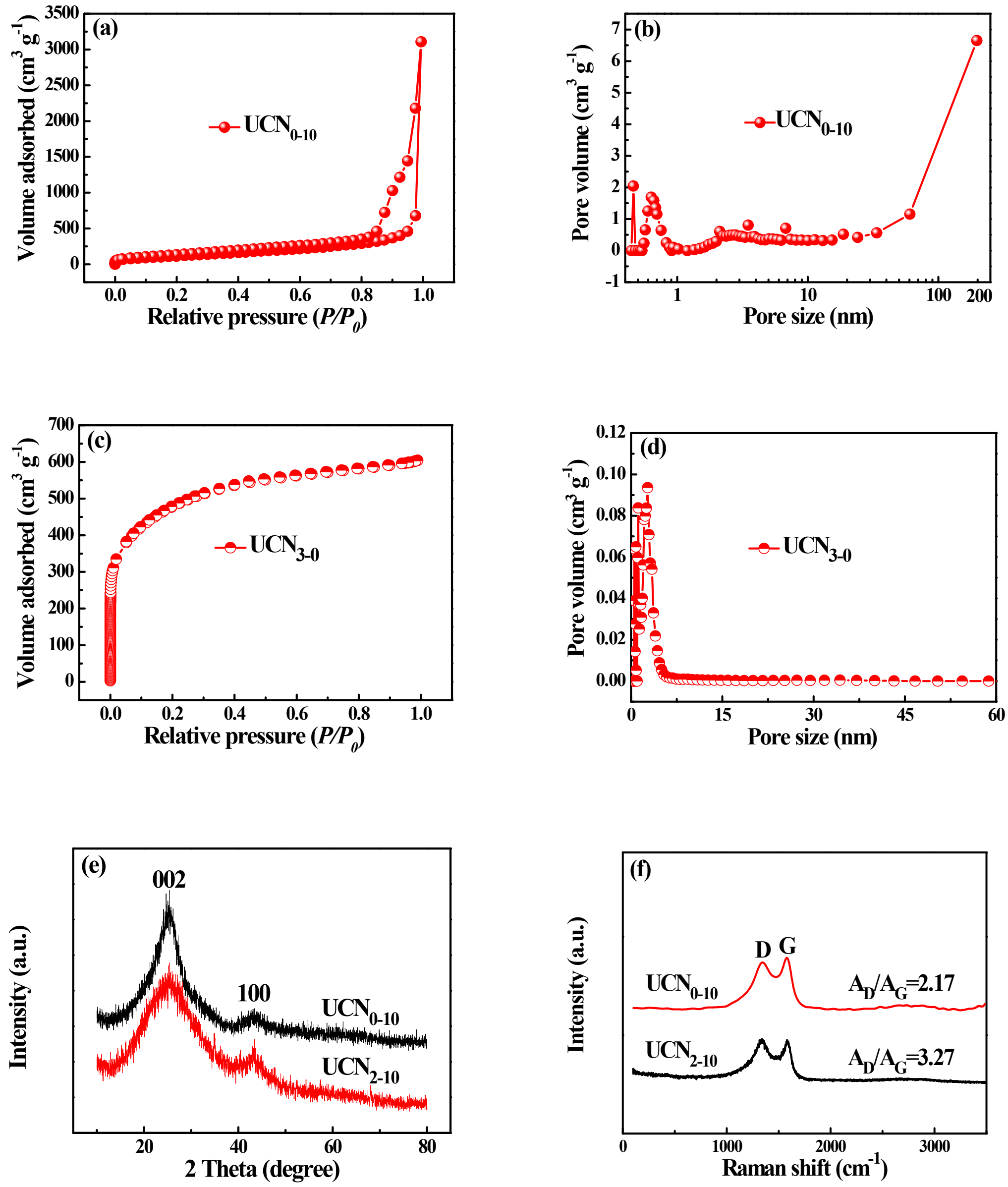


**Figure S4.** $N_2$ adsorption-desorption isotherms of: (a) $UCN_{0-10}$, (c) $UCN_{3-0}$. Pore size distribution curves of: (b) $UCN_{0-10}$, (d) $UCN_{3-0}$. (e) XRD patterns of $UCN_{0-10}$ and $UCN_{2-10}$. (f) Raman spectra of $UCN_{0-10}$ and $UCN_{2-10}$.

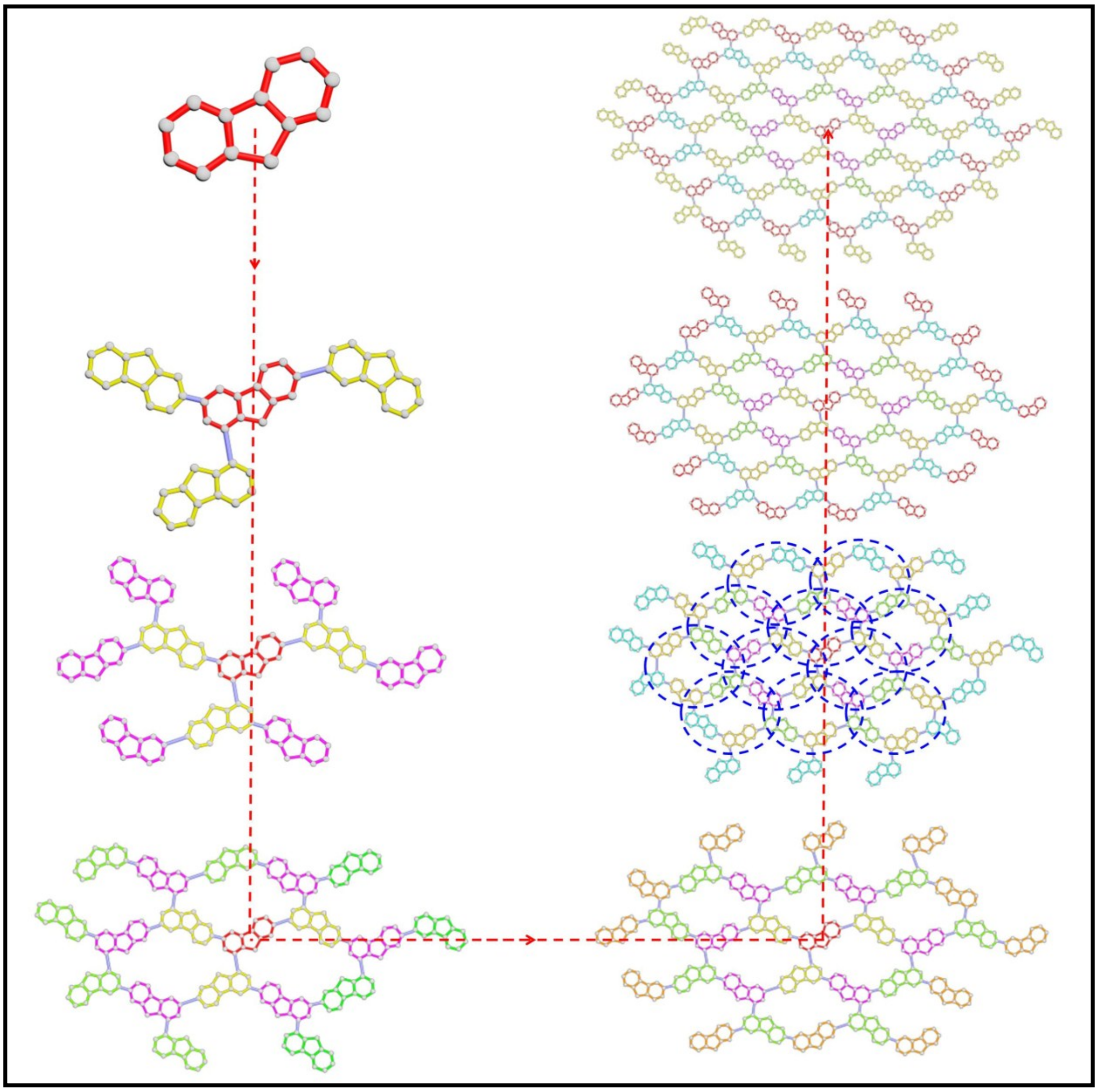

**Figure S5.** Carbon nanonets from fluorene molecules via step-by-step self-assembly process.

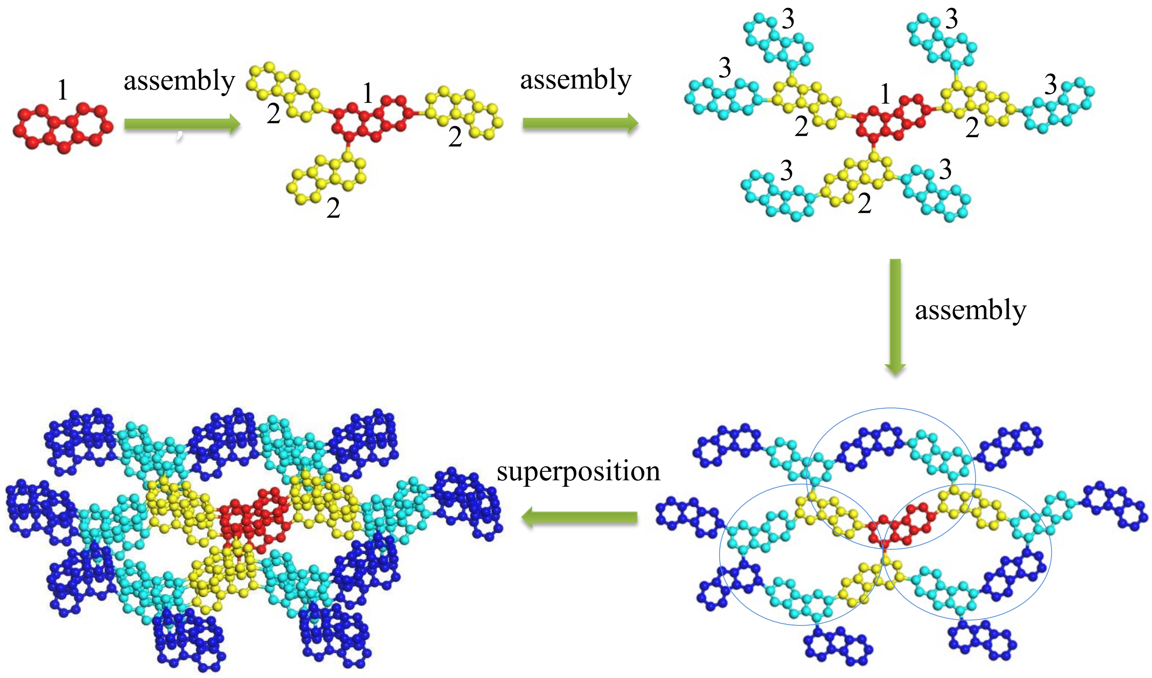


**Figure S6.** Schematic for the step-by-step assembly of six-membered fluorene rings.

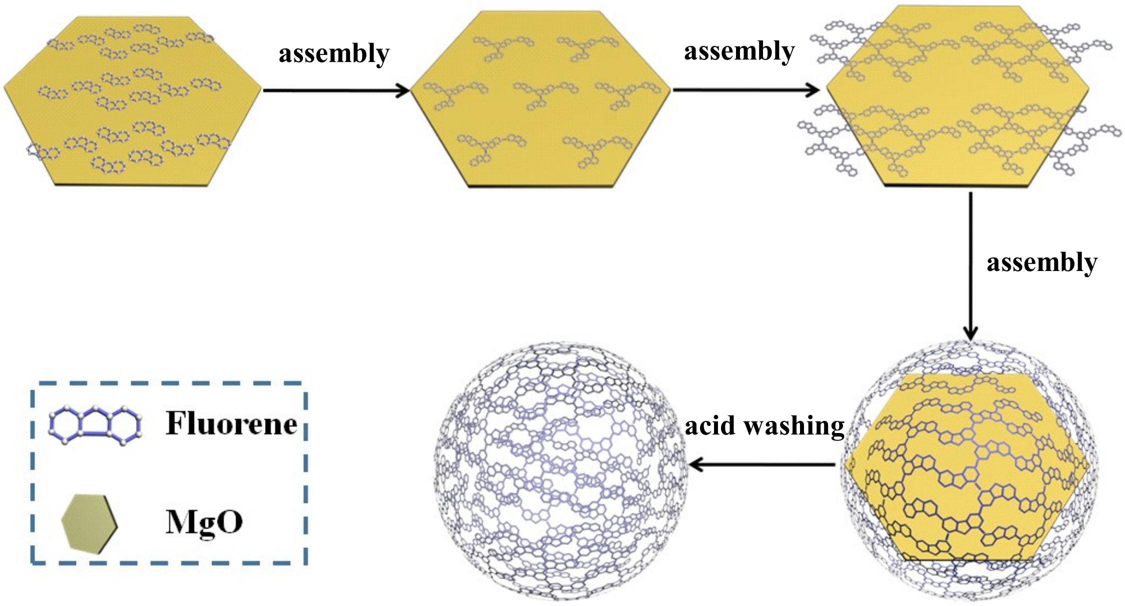


**Figure S7.** Schematic for the assembly of UCN from fluorene molecules.

**Table S1** The pore structure parameters of UCN samples.

| **Samples** | **BET surface area ($m^2$ $g^{-1}$)** | **Average pore diameter (nm)** | **Pore volume ($cm^3$ $g^{-1}$)** | **Micropore volume ($cm^3$ $g^{-1}$)** |
|---|---|---|---|---|
| $UCN_{0\text{-}10}$ | 461 | 41.7 | 4.81 | 0.04 |
| $UCN_{2\text{-}10}$ | 2107 | 2.31 | 1.21 | 0.88 |
| $UCN_{3\text{-}10}$ | 2550 | 2.40 | 1.57 | 1.06 |
| $UCN_{4\text{-}10}$ | 1581 | 2.24 | 0.88 | 0.68 |
| $UCN_{3\text{-}0}$ | 1701 | 2.20 | 0.94 | 0.25 |

**Table S2** The XPS results of the UCN samples.

| Samples | C1s (%) | O1s (%) | O1s | | |
|---|---|---|---|---|---|
| | | | C=O (%) | C-O (%) | O-H (%) |
| $UCN_{2-10}$ | 78.63 | 21.37 | 5.95 | 3.91 | 11.51 |
| $UCN_{3-10}$ | 89.52 | 10.48 | 5.35 | 5.13 | 0 |
| $UCN_{4-10}$ | 78.15 | 21.85 | 13.31 | 8.54 | 0 |

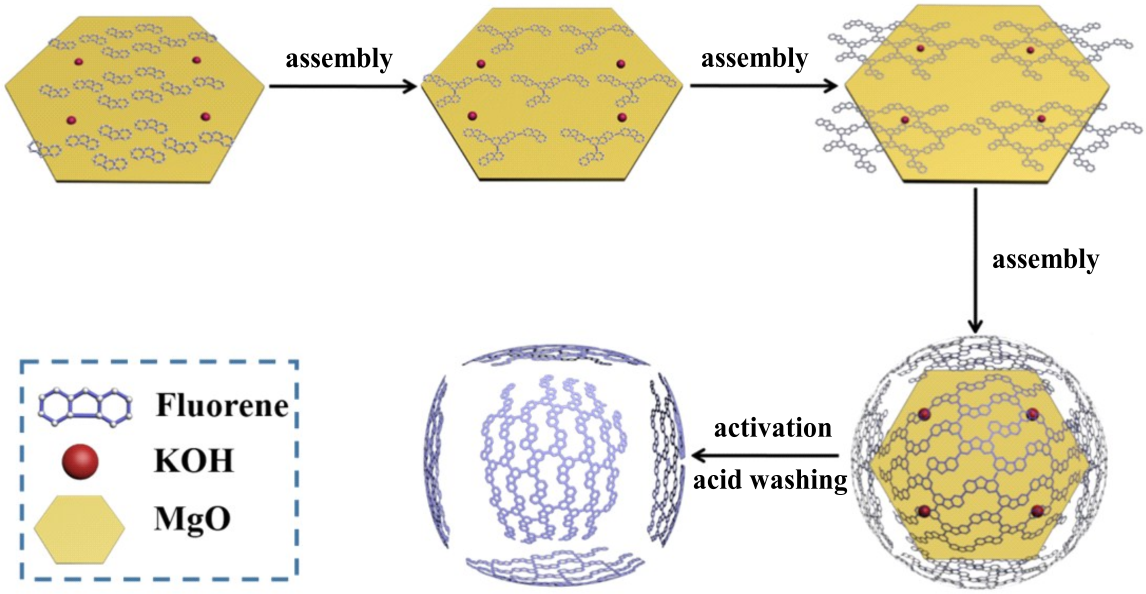


**Figure S8.** Schematic for the assembly of UCNs from fluorene molecules in nano-MgO-template-confinement space with the aid of KOH.

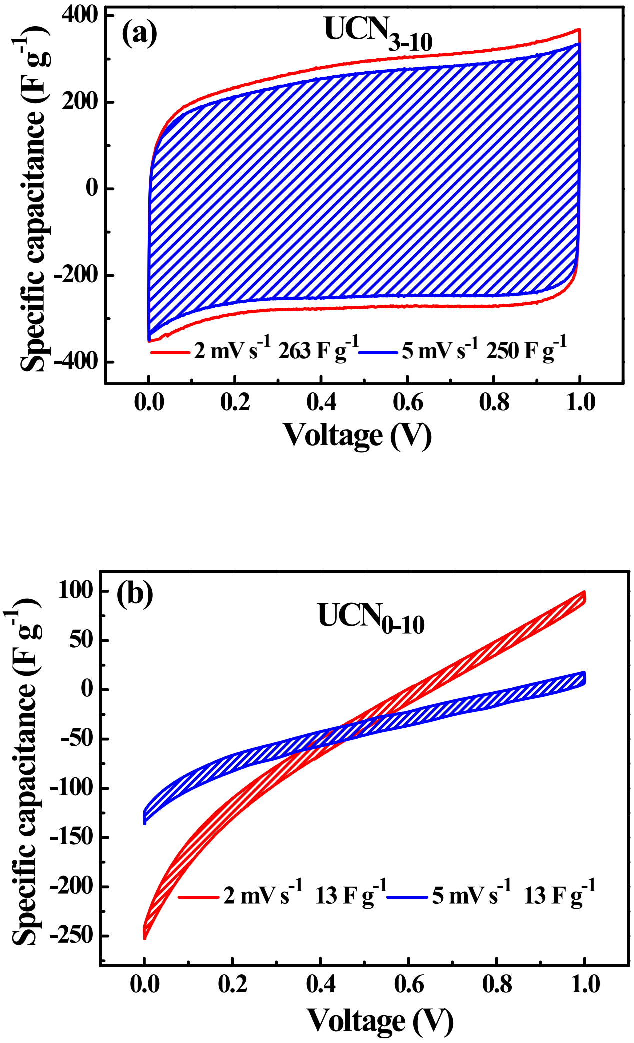


**Figure S9.** (a) CV curves of $UCN_{3-10}$ electrode at 2 and 5 mV $s^{-1}$. (b) CV curves of $UCN_{0-10}$ electrode at 2 and 5 mV $s^{-1}$.

**Table S3** Comparison of the specific capacitance of the UCN electrode with that of the hollow nanostructure carbons.

| Materials | Electrolyte | Current density (A $g^{-1}$) | Specific capacitance (F $g^{-1}$) | Ref. |
|---|---|---|---|---|
| BFC | 6 M KOH | 1.0 | 200 | 1 |
| CCNC1 | 6 M KOH | 0.1 | 205 | 2 |
| SRPC-4K-900 | 6 M KOH | 0.5 | 276 | 3 |
| HP-CF | 6 M KOH | 0.5 | 238 | 4 |
| NPC-m | 6 M KOH | 0.5 | 301 | 5 |
| HPCNC-700-a | 6 M KOH | 1.0 | 288 | 6 |
| HPCNFs-N | 6 M KOH | 1.0 | 307 | 7 |
| h-CNS900 | 6 M KOH | 0.1 | 272 | 8 |
| **$UCN_{3\text{-}10}$** | **6 M KOH** | **0.05**<br>**1.0** | **313**<br>**282** | **This work** |

**Table S4** Comparison of the performance of the UCN electrode with that of the carbon-based electrode materials.

| Materials | $S_{BET}$ ($m^2\ g^{-1}$) | Electrolyte | Current density ($A\ g^{-1}$) | $C_g$ ($F\ g^{-1}$) | Ref. |
|---|---|---|---|---|---|
| a-CBP | 1326 | 6 M KOH | 2 mV $s^{-1}$ | 296 | 9 |
| FPGF-200 | 7 | 6 M KOH | 0.5 | 388 | 10 |
| N-$ACN_{10}$ | 1630 | 6 M KOH | 2 mV $s^{-1}$ | 331 | 11 |
| TRGN | – | 6 M KOH | 2 mV $s^{-1}$ | 442.8 | 12 |
| a-PNC-10 | 434 | 6 M KOH | 2 mV $s^{-1}$ | 369 | 13 |
| S-3DCN | 575 | 6 M KOH | 1.0 | 395 | 14 |
| GSI/Ni | – | 6 M KOH | 0.2 | 236 | 15 |
| WPCNS | 1136 | 6 M KOH | 0.05 | 286 | 16 |
| **$UCN_{3-10}$** | **2550** | **6 M KOH** | **0.05**<br>**1.0** | **313**<br>**282** | **This work** |

References

1 F. Sun, Z. B. Qu, J. H. Gao, H. B. Wu, F. Liu, R. Han, L. J. Wang, T. Pei, G. B. Zhao and Y. F. Lu, Adv. Funct. Mater. 2018, 28, 180419.

2 Y. F. Bu, T. Sun, Y. J. Cai, L. Y. Du, O. Zhuo, L. J. Yang, Q. Wu, X. Z. Wang and Z. Hu, Adv. Mater. 2017, 29, 1700470.

3 N. N. Guo, M. Li, Y. Wang, X. K. Sun, F. Wang and R. Yang, ACS Appl. Mater. Interfaces, 2016, 8, 33626–33634.

4 J. Z. Chen, J. L. Xu, S. Zhou, N. Zhao and C.-P. Wong, Nano Energy, 2016, 25, 193–202.

5 X. W. Dong, Z. Yang, X. Wu, Y. S. Luo, T. Q. Chen, M. Li, N. T. Hu and Y. F. Zhang, Electrochim. Acta, 2017, 251, 263–269.

6 J. Q. Shao, M. Y. Song, G. Wu, Y. H. Zhou, J. F. Wan, X. Ren and F. W. Ma, Energy Storage Mater. 2018, 13, 57–65.

7 L.-F. Chen, Y. Lu, L. Yu and X. W. Lou, Energy Environ. Sci., 2017, 10, 1777–1783.

8 Q.-L. Zhu, P. Pachfule, P. Strubel, Z. P. Li, R. Q. Zou, Z. Liu, S. Kaskel and Q. Xu, Energy Storage Mater., 2018, 13, 72–79.

9 C. L. Long, D. P. Qi, T. Wei, J. Yan, L. L. Jiang and Z. J. Fan, Adv. Funct. Mater., 2014, 24, 3953–3961.

10 L. L. Jiang, L. Z. Sheng, C. L. Long, T. Wei and Z. J. Fan, Adv. Energy Mater., 2015, 5, 1500771.

11 Q. H. Zhou, J. Chang, Y. T. Jiang, T. Wei, L. Z. Sheng and Z. J. Fan, Electrochim. Acta, 2017, 251, 91–98.

12 X. L. Wu, D. R.Yang, C. K. Wang, Y. T. Jiang, T. Wei and Z. J. Fan, Carbon, 2015, 92, 26–30.

13 Q. Wang, J. Yan, Y. Xiao, T. Wei, Z. J. Fan, M. L. Zhang and X. Y. Jing, Electrochim. Acta, 2013, 114, 165–172.

14 X. Y. Deng, S. Zhu, J. J. Li, F. He, E. Z. Liu, C. N. He, C. S. Shi, Q. Y. Li, L. Y. Ma, N. Q. Zhao, Carbon, 2019, 143, 728–735.

15 G.-H. An and H. J. Ahn, Appl. Surf. Sci., 2019, 473, 77–82.

16 H. F. Zhang, X. J. He, J. Gu, Y. Y. Xie, H. F. Shui, X. Y. Zhang, N. Xiao and J. S. Qiu, Fuel Process. Technol., 2018, 175, 10–16.